Identifying Heterogeneous Friction Coefficients on the Hot Forming Tools in Mannesmann Cross-Roll Piercing

Meriane Fernandes, Nabil Marouf, Pierre Montmitonnet, Katia Mocellin

Identifying heterogeneous friction coefficients on the hot forming tools in Mannesmann cross-roll piercing

FERNANDES Meriane[1,a *], MAROUF Nabil[1,b], MONTMITONNET Pierre[2,c] and MOCELLIN Katia[2,d]

[1] Vallourec Research Centre France, Aulnoye-Aymeries, 59620, France

[2] CEMEF, MINES ParisTech, PSL*, CNRS UMR7635, Sophia Antipolis, 06904, France

[a]meriane.fernandes@vallourec.com, [b]nabil.marouf@vallourec.com , [c]pierre.montmitonnet@mines-paristech.fr , [d]katia.mocellin@mines-paristech.fr

* corresponding author

Keywords: Tube piercing ; Mannesmann process ; Roll grinding ; Non-uniform friction.

Abstract. The effect of friction on all the tools of the Mannesmann cross-roll piercing process is investigated numerically. The friction between billet and cross rolls is a driving force on the first half of the rolls and may become resistant on the downstream part depending on process settings. The friction between piercer plug and hot metal is of course resistant. Friction on rotating Diescher guide disks is driving in the piercing direction, but resistant in the rotation direction; if static (pure sliding) lateral guide shoes are preferred, friction is resistant in both directions. Friction on the upstream part of rolls must therefore be as high as possible for correct entrainment and process stability, which explains the practice of knurling it to very high roughness. The surface of the piercer plug must be smooth. The surface states of guides and of the downstream half of rolls are free setting parameters. The effects of the different friction coefficients on entrainment speed and state of stress are quantitatively evaluated using the 3D Finite Element Method (FEM, ForgeNxT). Results suggest how estimates of friction coefficients can be obtained by comparing with observables on the mill.

Introduction

Tube piercing is the first step of seamless tube manufacturing, followed by different kinds of rolling processes to expand the tube, reduce its wall thickness and/or its diameter [1]. In the Mannesmann cross-roll piercing mill (schematically pictured in Fig. 1), a full hot cylindrical billet is given a helical movement by two conical rolls with axes offset by the *feed angle* (a few degrees), thus being pushed against a fixed plug ahead of which high triaxiality opens a cavity through ductile damage mechanisms. The cavitated billet is then formed into a hollow shell by the piercer plug, with the help of two lateral tools which restrain the ovalization of the hollow shell (either static guiding shoes or rotating *Diescher guide rolls*); in a transverse section, these guides have a circular groove, the radius of which is somewhat larger than the tube radius.

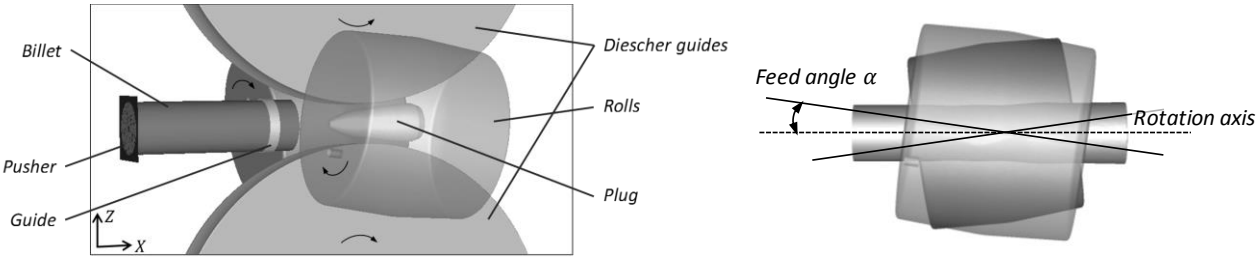

Figure 1: schematic configuration of a cross-roll piercing mill

The complexity of this process makes numerical simulation highly desirable to understand its kinematics and mechanics and help design the tooling and procedures by disclosing the consequences of the choices on tube geometrical and metallurgical quality. Therefore, quite a few 3D FEM studies

have been published in the last two decades, starting with Komori [2] who focused on the steady-state phase of the process. They deal mainly with prediction of the cavity opening by the Mannesmann effect and with the final metallurgical state of the metal using criteria such as maximum temperature or ductile damage models. Of particular importance is the position of the tip of the plug with respect to the minimum gap point between the rolls (called rolls high point, or HP) [3]: too far upstream, the crack does not open, the separation of the metal occurs at the tip of the plug which is severely worn; too far downstream, the crack surface has been left enough time to oxidize and an internal surface defect is formed. Ceretti et al. modelled crack opening using a Latham and Cockroft ductile damage model [4,5]. In the following years, Fanini and coworkers produced an in-depth study of the Mannesmann effect [6-10], explained it by the occurrence of a tensile stress in the direction normal to the compression by the rolls in the cross section. They focused on the onset of crack opening mechanism and therefore omitted the piercer plug in their simulations for simplicity. Comparing several ductile damage models, they finally advocated a version of the Lemaitre model [8] and emphasized the impact of pre-existing porosity due to casting [6,9] or more generally of any metallurgical weakness or brittleness of the centreline of the billet. Starting from this conclusion, Skripalenko and coworkers recently studied the effect of the plug shape and more generally of the tooling on final shell porosity [11-12]; among the damage models, they promoted the normalized Latham and Cockroft one [13]. Romanenko and coworkers [14-15], Zhang et al. [16] chose maximum temperature as an indicator of success of the process and metallurgical quality of the shell.

However, oversimplified friction models have been applied systematically, namely constant and uniform friction on all tools. Yet, friction plays a major and multiform role in this process. Friction between billet and conical rolls must be high enough to entrain the billet, all the more as friction on the piercer plug resists tube advance. The plug mounted on its bar is free in rotation, so that only its friction component in the piercing direction is of interest. Finally, whereas sliding friction on guide shoes is purely resistant, Diescher disks are rotating fast enough that friction pushes the tube forward.

The possibility of rolling is therefore primarily a balance between the resistance force due to plug friction and the driving force brought by conical rolls and Diescher disks friction. Engagement problems are often met, solved in practice by giving the upstream half of the rolls (at least) a very large roughness, thus maximizing friction [3]. High friction also enhances tensile triaxiality on billet axis, induced by the small diameter reduction imparted by the rolls (the aspect ratio, diameter / contact length, is high). On the contrary, the downstream half of the rolls, which controls expansion over the plug, and the plug itself may be given a smoother surface state to moderate resisting force.

In the present paper, numerical simulation is used to understand in details the role and effects of friction non-uniformity on the different tools, with special emphasis on the tube exit velocity to check the entrainment capacity of the process. Based on this and available experimental observables, a strategy is proposed to identify the range of friction coefficients prevailing in each of the contacts.

Brief description of the FEM model

Tool design. The configuration is depicted in Fig. 1. Billet dimensions are ϕ120 mm x L400 mm. The rolls are barrel-type with maximum diameter ϕ_{rolls} = 420 mm; inlet and outlet cone angles are respectively 3° and 4°. Diescher disks (ϕ_D = 955 mm) are used as lateral guides. The minimum gap between cross rolls is 105 mm and their feed angle is α = 8°. The distance between Diescher disks is 120 mm, aiming at a final tube outer diameter (OD) ~130 mm. Imposed rotational velocities are respectively ω_{rolls} = 80 rev / min (8.38 rad.s^{-1}) and ω_D = 12 rev / min (1.25 rad.s^{-1}). The plug has a maximum diameter of 94 mm, its tip position is 73 mm ahead of the minimum cross roll gap (HP). It is modelled as a "floating tool" in the orthoradial direction, i.e. a zero torque condition is applied and its rotational velocity is an output of the simulation. It has no translational degree of freedom

FE discretization. All the tools are rigid. Their typical mesh size (triangular facets) is around 8 mm. As for the billet, the 4-node tetrahedron "mini-element" is used [17]. The "bimesh" option is activated [18]: the temperature field is calculated with a fine mesh everywhere (6 mm) whereas mechanical equations are solved with a de-refined mesh (up to a factor 4) outside of a predefined

volume encompassing the plastic deformation zones. Remeshing is triggered once a deformation equal to 1 is locally reached. The computing time step is automatically chosen by the software in the interval 10^{-3} – 10^{-1} s, based on velocity and temperature evolution and on convergence statistics.

Constitutive model. The billet is made out of S355 steel (0.27 w% C, 0.55 w% Si, 1.6 w% Mn) austenitized at 1240°C for 90 minutes. A pure viscoplastic law (Norton-Hoff) is assumed, the strain, temperature and strain rate dependence is pictured in Fig. 2. It has been checked that an elastic-viscoplastic behavior does not significantly change the results.

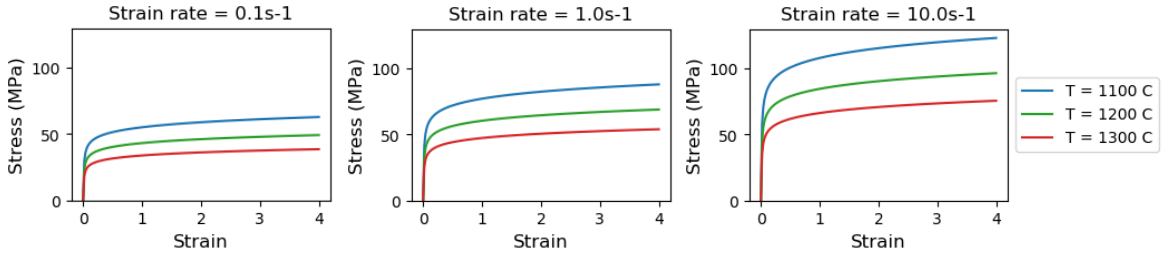

Figure 2: Constitutive model chosen for S355 steel

Contact and friction. The non-penetration condition is approximately enforced using a penalty technique [17]; the penetration is always observed to be maintained below 0.01 mm.

Friction is described by the Tresca model $\tau = \bar{m}\bar{\sigma}/\sqrt{3}$ where τ is the friction stress and $\bar{\sigma}$ is von Mises equivalent stress. The standard case is $\bar{m}_R = 1$ on the cross rolls, $\bar{m}_{plug} = 0.3$ on the piercer plug and $\bar{m}_D = 0.45$ on the other tools. Parametric tests varying these values are described below.

Thermal transfer. The initial billet temperature is taken uniform at 1240°C (furnace temperature); attempts with a radial temperature gradient resulting from a cooling stage did not change results significantly and is omitted here for the sake of brevity as well as clarity.

Based on measurements on the mill, cross rolls and Diescher disks are given a temperature of 80°C, whereas the plug is given its estimated average temperature during one piercing, i.e. 500°C.

The Heat Transfer Coefficients are taken the same on all tools, h = 10 kW.m^{-2}.K^{-1}. Frictional heat partition is made according to the ratio of effusivities, i.e. practically ½ (steel / steel contact).

Standard friction case

The standard case corresponds to a uniform friction on rolls, $\bar{m}_R = 1$. In this case, the final computed OD is ~128 mm and the load calculated on cross rolls, Diescher guides and piercer plug are respectively 620, 100 and 200 kN. The output speed of the tube v_{output} is 214 mm.s^{-1}. In order to evaluate the efficiency of the process and the rolls capacity to push the billet forward, a ratio is introduced, feed efficiency E_{feed}, normalizing the output speed by the maximum axial speed of rolls:

$$E_{feed} = \frac{v_{output}}{\pi \times \emptyset_{\text{rolls}} \times \sin(\alpha) \times \omega_{rolls}} \qquad (= 0.88 \text{ for } v_{output} = 214 \text{ mm.s}^{-1}) \qquad (1)$$

Figure 3b shows two successive high pressure contact zones. The first one (on the left of the picture) corresponds to the initial compression by the upstream half of the cross rolls (convergence angle 3°). Then the pressure drops at the entry of the diverging, downstream part of the rolls where the gap opens due both to the exit barrel angle (4°) and to the roll crossing (feed angle 8°). But at the same time the plug is expanding the tube and eventually presses it and against the Diescher disks in the xOy plane and against the downstream half of the rolls in the xOz plane: hence the second high pressure zone. This pressure profile strongly depends on the plug profile and position.

In this whole contact area between rolls and billet, the billet velocity in the feed direction (x-axis) and its rotational speed are both everywhere smaller than the corresponding cross roll speeds, respectively 244 and 1742 mm.s^{-1} (see Fig. 3a and Fig. 3c). This means that the billet is drawn by rolls but, due to the resistance opposed by the piercer plug, it is everywhere in a condition of backward slip, there is no neutral line. This also explains why severe entrainment problems are often met, requiring special treatment [3]. Moreover, x-velocity is very heterogeneous in the inlet zone, the

metal in contact with the cross rolls and Diescher disks is strongly pushed forward, whereas the rest of the section is slowed down by the contact with the piercer plug. Further downstream, reduction of the section around the plug causes a sudden acceleration in the feed direction.

The rotational velocity is complex as well (Fig. 3c). At entry it is ~ 1600 – 1610 mm.s^{-1}. It drops to ~1550 mm.s^{-1} and becomes very θ-heterogeneous as the billet gets oval in the first contact zone (rolls upstream part). Then it reaccelerates up to ~1660 mm.s^{-1} as tube radius re-grows under rolls downstream part due to the expansion by the plug. This deceleration / acceleration results in a slight positive then negative torsion ; in the end, a generator of the billet remains almost straight (Fig. 3d).

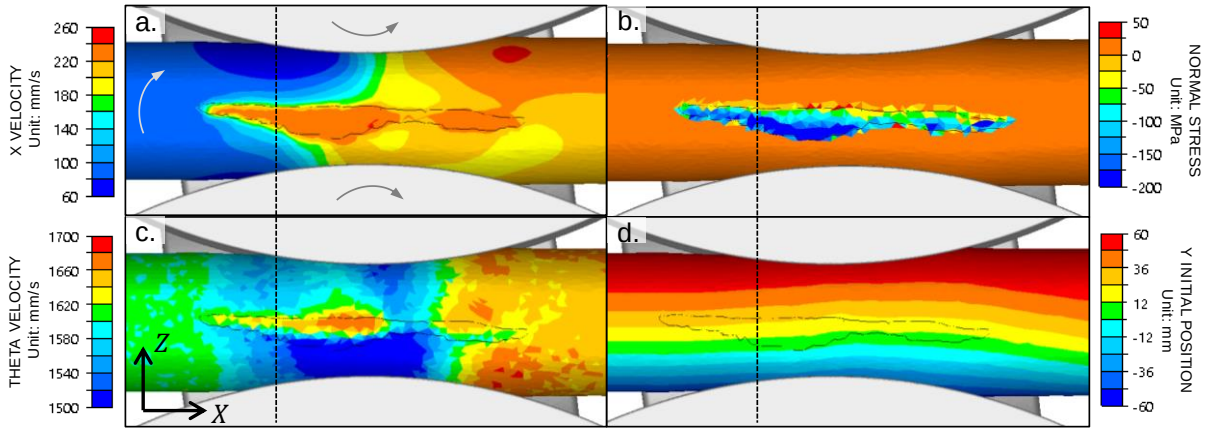

Figure 3: assessment of friction effects from computed field variables, uniform roll friction ($\overline{m}_R = 1$ everywhere). The contact zone boundary is outlined in black. The dotted vertical line represents the position of the tip of the plug. From left to right and top to bottom: axial velocity field of the billet; contact pressure field; rotational velocity field of the billet; twisting of the billet under the rolls (the variable is the initial position of each material point on the vertical axis).

Impact of non-uniform friction

In order to determine the effect of a non-uniform cross rolls surface state, the standard case is compared to a second one where rolls are given high friction on their upstream part ($\overline{m}_{R,up} = 1$) and smoother surface on their downstream part ($\overline{m}_{R,down} = 0.45$).

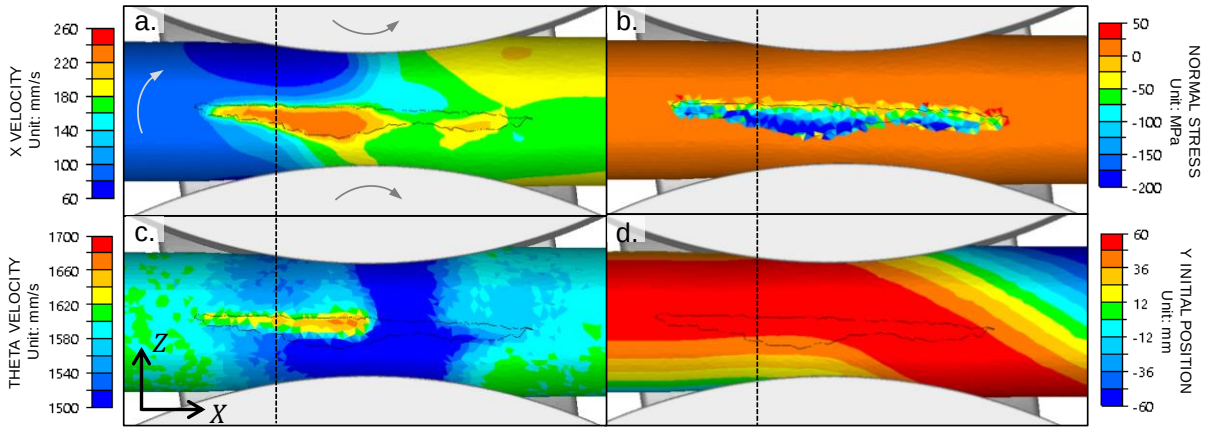

Figure 4: assessment of friction effects from computed field variables: non-uniform roll friction ($\overline{m}_{R,up} = 1, \overline{m}_{R,down} = 0.45$). Compare with the same variables in Fig. 3.

The feed efficiency is much lower, E_{feed} = 0.75 vs 0.88 for the standard case. This means that a high $\overline{m}_{R,down}$ also has a significant positive impact on the exit velocity and participates in the pushing force. Yet, the contact pressure is almost the same (Fig. 3b. vs 4b). The axial velocity is the same on the entry side, but is of course lower on the exit side; the second high v_x zone is much less visible due to lower friction, unable to impose the same amount of shear (Fig. 4a). The same applies

to the rotation: $\bar{m}_{R,down}$ is too low to compensate the resistance to rotation due to the Diescher disks so that the second, inverse torsion almost disappears (Fig. 4c), resulting in a large twist of the shell (Fig. 4d), the most conspicuous difference which is indeed a practical indicator in the workshop.

Considering the evidence of the impact of $\bar{m}_D$, other simulations have been run with $\bar{m}_D = 0$ (i.e. Diescher disks just control ovalization but apply neither a pushing force in the axial, nor a resisting torque in the rotation direction). Results (not shown) disclose insignificant impact if cross roll friction is uniform ($\bar{m}_{R,down} = \bar{m}_{R,up} = 1$) ; if $\bar{m}_{R,down} = 0.45$, no impact of $\bar{m}_D = 0$ on axial velocity and E_{feed}, but a ~5% increase of rotational velocity; as a consequence, twist considerably decreases.

Discussion: identification of friction coefficients

The study has been extended to $0.2 \leq \bar{m}_{plug} \leq 0.45$ and $0.2 \leq \bar{m}_{R,down} \leq 1$ (with $\bar{m}_D = 0.45$). Results on E_{feed} and shell twist angle are presented in Fig. 5. E_{feed} depends both on the resistant force on the plug, proportional to $\bar{m}_{plug}$, and on cross rolls driving force. The latter grows with both $\bar{m}_{R,up}$ and $\bar{m}_{R,down}$: due to the absence of a neutral line, friction is a driving force everywhere in the rolls / billet contact, with the only exception of $\bar{m}_{plug} \sim 0$. E_{feed} does not depend on Diescher friction $\bar{m}_D$. Twist depends strongly on $\bar{m}_{R,up}$ - $\bar{m}_{R,down}$ and $\bar{m}_D$, but not on $\bar{m}_{plug}$ which does not resist rotation. The exit rotation velocity (in rad.s^{-1}) increases with $\bar{m}_{R,down}$ but decreases when $\bar{m}_D$ grows.

Twist and angular velocity are strongly correlated, and so are $\bar{m}_{R,up}$ - $\bar{m}_{R,down}$ and $\bar{m}_D$. This means another observable is necessary to determine all three $\bar{m}_{R,down}$, $\bar{m}_D$ and $\bar{m}_{plug}$ (assuming $\bar{m}_{R,up}$ is forced to 1). This could be e.g. the torque on the Diescher disks, very sensitive to $\bar{m}_D$ and little to the others. Alternatively, ensuring $\bar{m}_{R,down} = 1$ would leave two coefficients for two independent observables, twist depending on $\bar{m}_D$ and not on $\bar{m}_{plug}$ and the opposite for E_{feed}.

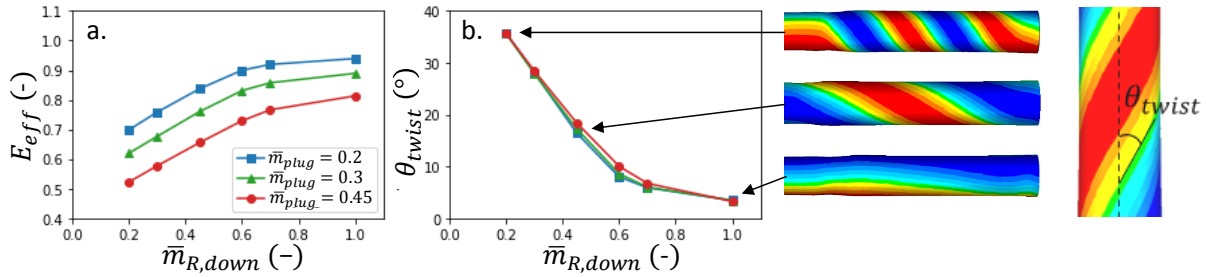

Figure 5: effects of the piercer plug and cross rolls friction coefficients on two practical observables, feed efficiency (a.) and twist angle (b.)

Conclusion

This study of cross-roll piercing tribology has shown that kinematics and even plastic flow (torsion) are quite sensitive to friction coefficients and even their heterogeneity on a single tool. On the contrary, little effect has been found on tube external geometry, i.e. ID / OD and tube thickness. Different effects on different observables allow estimating all those coefficients. Furthermore, insight has been gained on the whole behaviour of this complex system; tool surface engineering can be redesigned based on this.

References

[1] K.-H. Brensing and B. Sommer, Steel Tube and Pipe Manufacturing Process, Available at: https://pdfs.semanticscholar.org/1e72/45a6f6c8e88a7db893d5b311feb5f8083d7d.pdf?_ga=2.94978270.356729499.1577025450-670639474.1577025450.

[2] K. Komori, Simulation of Mannesmann piercing process by the three-dimensional rigid-plastic finite-element method, Int. J. Mech. Sci., 47, 12 (2005) 1838–1853.

[3] E. Ceretti, 2D Simulation and validation of rotary tube piercing process, in : S. Ghosh, J. C. Castro and J. K. Lee (Eds), Proc. NUMIFORM 2004 (Colombus, OH, USA, 13-15 June 2004), AIP Conference Proceedings, vol. 712, pp. 1154–1159.

[4] E. Ceretti, C. Giardini, and F. Brisotto, Development of a simulation model of the rotary tube piercing process and FEM application to improve the quality of seamless tubes, in : P. Bariani (Ed), Proc.8th Int. Conf. Tech. Plast. (Verona, Italy, 9-13 October 2005), pp. 281-282.

[5] E. Ceretti, C. Giardini, and A. Attanasio, 3D Simulation and validation of tube piercing process, in : J.M.A. Cesar de Sa and A.D. Santos (Eds), Proc. NUMIFORM 2007 (Porto, Portugal, 17-21 June 2007), AIP Conference Proceedings, vol. 908, pp. 413–418.

[6] S. Fanini, A. Ghiotti, and S. Bruschi, Evaluation of fracture initiation in the Mannesmann piercing process, in: E. Cueto, F. Chinesta (Eds), Proc. 10th Esaform Conf. (Zaragoza, Spain, 18-20 April 2007), AIP Conference Proceedings, vol. 907, pp.709–714.

[7] S. Fanini, A. Ghiotti, and S. Bruschi, Prediction of the fracture due to Mannesmann effect in tube piercing, in : J.M.A. Cesar de Sa and A.D. Santos (Eds), Proc. NUMIFORM 2007 (Porto, Portugal, 17-21 June 2007), AIP Conference Proceedings, vol. 908, pp. 1407–1412.

[8] Y. Chastel, A. Diop, S. Fanini, P.-O. Bouchard, and K. Mocellin, Finite element modeling of tube piercing and creation of a crack, in : P. Boisse, F. Morestin, E. Vidal-Sallé (Eds), Proc. 11th ESAFORM Conference (Lyon, France, 23-25 April 2008), vol. 1, pp. 355-358.

[9] S. Fanini, Modelling of the Mannesmann effect in tube piercing, PHD Dissertation, Università degli Studi di Padova, 2008.

[10] A. Ghiotti, S. Fanini, S. Bruschi, and P.F. Bariani, Modelling of the Mannesmann effect, CIRP Ann., 58, 1 (2009) 255–258.

[11] M.M. Skripalenko, V.E. Bazhenov, B.A. Romantsev, M.N. Skripalenko, T.B. Huy, and Y.A. Gladkov, Mannesmann piercing of ingots by plugs of different shapes, Mater. Sci. Technol. 32, 16 (2016) 1712–1720.

[12] B.A. Romantsev, M.M. Skripalenko, T.B. Huy, M.N. Skripalenko, Y.A. Gladkov, and A.A. Gartvig, Computer simulation of piercing in a four-high screw rolling mill, Metallurgist, 61, 9–10 (2018) 729–735.

[13] M.M. Skripalenko, B.A. Romantsev, S.P. Galkin, M.N. Skripalenko, L.M. Kaputkina, and T.B. Huy, Prediction of the fracture of metal in the process of screw rolling in a two-roll mill, Metallurgist, 61, 11–12 (2018) 925–933.

[14] V.P. Romanenko, P.L. Alekseev, E.A. Kharitonov, A.A. Yandimirov, and A.A. Sevastyanov, Study of the temperature regimes in the heating and piercing of steel ingots to obtain thick-walled shells, Metallurgist, 55, 1–2 (2011) 28–33.

[15] V.P. Romanenko and D.V. Sizov, Evaluating the adequacy of a mathematical model of the piercing of a billet into an ultra-thick-walled shell on a two-high rotary rolling mill, Metallurgist, 57, 9–10 (2014) 830–836.

[16] Z. Zhang, D. Liu, Y.H. Yang, Y. Zheng, Y.H. Pang, J.G. Wang and H.P. Wang, Explorative study of rotary tube piercing process for producing titanium alloy thick-walled tubes with bi-modal microstructure, Arch. Civ. Mech. Eng., 18, 4, (2018) 1451–1463.

[17] L. Fourment, J.-L. Chenot and K. Mocellin, Numerical formulations and algorithms for solving contact problems in metal forming simulation, Int. J. Num. Meth. Engg 46, 9 (1999) 1435-1462

[18] M. Ramadan, L. Fourment, H. Digonnet, Fast resolution of incremental forming processes by the Multi-Mesh method. Application to cogging, Int. J. Mater. Forming 7, 2 (2014) 207-219